Nascent Rotational Distribution of $CO_2(00^0 0, J)$ States from Collisions with Highly Vibrationally Excited Na_2

X.F. Zhao, Z.L. Yu, S.Y. Wang*, C. Qin, Y.F. Shen and K. Dai

School of Physical Sciences and Technology, Xinjiang Key Laboratory of Solid State Physics and Devices, Xinjiang University, No. 777 Huarui Street, Shuimogou District 830046, Urumqi, China

In this work, the high vibrational states of Na_2 were excited via stimulated emission pumping. The full-state resolution distribution of molecular scattering of $CO_2(00^0 0, J)$, resulting from collisions with excited Na_2 $X^1\Sigma_g^+$ ($v'' = 33$ and 45), was also investigated. In particular, the scattered $CO_2(00^0 0, J = 2\text{--}80)$ molecules were found to possess a biexponential rotational distribution. The low- and high-energy distributions were derived by fitting the data by means of a biexponential model. The cold distribution accounted for 80% of the total scattering and was caused by elastic or weakly inelastic collisions. Such collisions might have caused very small rotational excitations in CO_2. The hot distribution involved substantial changes in the rotational energy of CO_2 and accounted for 20% of the total amount of collisions. The influence of the donor energy on the rotational distribution was shown to be very large; however, for the two types of donor energies, the branches associated with inelastic and elastic collision rates were the same. The nascent translational energy curves for scattered $CO_2(00^0 0, J = 56\text{--}80)$ were measured via high-resolution transient overtone fluorescence. For every 25% enhancement in donor vibrational energy, the product translational energy of an individual J-state increased by 60%. Additionally, the measured collision rates were found to be weakly dependent on the donor energy.

topics: spectroscopy measurement, energy transfer, stimulated emission pumping, excited Na_2

1. Introduction

The scientific understanding of the excited state structure of atoms and molecules not only provides a detailed and reliable experimental basis for theorists but also plays a key role in promoting the development of quantum chemistry, chemical reaction dynamics, and other related disciplines. Thus, a suitable understanding of the molecular energy transfer processes is urgently required in many science and technology fields, including laser chemistry [1], biochemistry [2], applied physics [3], plasma physics [4], aviation technology, and even astronomy [5].

Collisions between highly vibrationally excited molecules (when the internal energy approaches the dissociation limit) and thermal bath molecules play an important role in the breakdown or rearrangement of molecules. The competition between the collisional energy transfer and the reaction determines the chemical reaction kinetics as a whole, as well as the dynamics, thereby affecting many associated atmospheric reactions [6–8] and combustion processes [9].

Numerous spectroscopic approaches relying on ultraviolet (UV) absorption [10], infrared (IR) fluorescence [11], overtone absorption [12], ultrafast transient absorption [13], and optical–optical double resonance [14] have been used to measure the high-energy collisional inactivation of molecules. In particular, the full-state resolved distribution of the nascent energy absorption in hot-bath molecules was analyzed by Mullin's group [15–17] using state-resolved transient spectroscopy. It has been shown that the energy transfer between CO_2 and pyrazine (with $E = 32700$ and 37900 cm^{-1}) mainly occurs through a vibration-to-rotation/translation (V-RT) channel. The nascent translational energy produced by the collision is very sensitive to the pyrazine energy. For example, a 16% increase in the pyrazine vibrational energy leads to a 50% increase in the recoil energy of the scattered molecules.

According to the biexponential rotational distribution of scattered CO_2 molecules, the majority of the collisions are weakly inelastic collisions (77%), and the rest are strongly inelastic collisions (23%). Compared with weak collisions, the distribution of strong collisions is sensitive to the changes in the donor E. Using stimulated Raman pumping to ex-

cite H_2 ($v = 1$), Shen's group [18] showed that high-energy donor molecules release more translational energy to the bath. They found that the translational energy increased by 120% when the donor energy was increased by 13%, suggesting that the nascent translational energy of LiH $(0, J)$ is sensitive to the H_2 energy. The results also showed that the overall appearance and depletion rate of H_2 at the two different energies were similar, demonstrating that the collision rate constant does not vary with the donor energy. Cui and colleagues [19] found that CO_2 is an efficient relaxation partner for the high vibrational states of KH. They used overtone pumping to excite KH to $v = 14$–21 and collide with CO_2, proving that when the internal energy of KH is increased by a factor of 1.27, the average rotational energy of CO_2 increases by a factor of nearly 1.35. The rate coefficient $k_{v''}(CO_2)$ depends strongly on the vibrational quantum number of KH, and the mean translational energy of scattered CO_2 molecules increases roughly linearly with the change in the J state of CO_2. In the present study, the collisional energy transfer of highly vibrationally excited Na_2 was experimentally measured in a CO_2 bath. A pump–probe technique was employed to obtain highly vibrationally excited Na_2 in its electronic ground state excited to rovibrational states $X^1\Sigma_g^+$ ($v'' = 33$, $J'' = 11$) and $X^1\Sigma_g^+$ ($v'' = 45$, $J'' = 11$) [20], and laser-induced fluorescence (LIF) was used to determine the vibrational states of the system under consideration.

2. Experimental methods

Under single-collision conditions, the rotational states of $CO_2(00^00)$ were excited by high overtones and detected using LIF. Despite the fact that the $CO_2(00^00, J)$ states were not detected via transient absorption, they could be identified through the following overtone excitation via LIF. The high resolution of the laser allowed us to measure the population of the individual rotational states in the scattered $CO_2(00^00)$ molecules. The rate measurements were conducted for both depletion and appearance of the population in the individual $CO_2(00^00, J)$ states.

A schematic of the experimental setup used in this work is shown in Fig. 1. The reaction cell consists of a five-armed crossed heat-pipe oven, in which four arms form a planar cross, while the perpendicular fifth arm, which contains the Na reservoir, is sealed at the base of the intersection of the four arms. The cell is connected to a vacuum instrument through a gas-supplying system that fills the pool with gas at different pressures under vacuum. During the experiment, the Na metal was heated in the bottom reservoir to a temperature between 450 and 900 K. The temperature of the cell was monitored by means of an intrusive thermocouple in
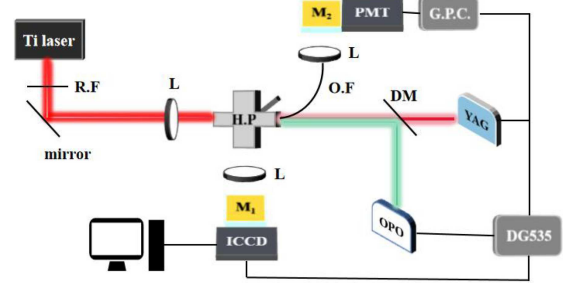

Fig. 1. Experimental setup: H.P — heat pipe oven; OPO — optical parametric oscillator; M — monochromator; PMT — photomultiplier; G.P.C — gated photon counter; DM — dichroic mirror; L — lens; DG535 — pulse delay box; R.F — removable filter; O.F — optical fiber.
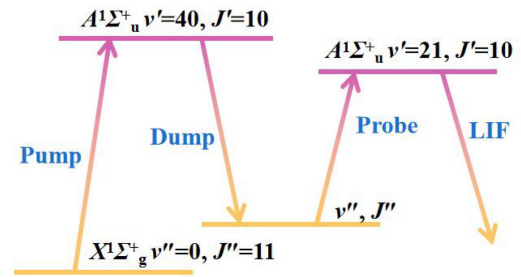

Fig. 2. Energy diagram of the pump–dump and probe scheme.

the vicinity of the collision regime. The CO_2 pressure in the cell was 15 mTorr. The cell was filled with CO_2 gas, which served both as a collision partner for the excited Na_2 molecules and as a buffer gas, preventing Na condensation on the cell windows.

Figure 2 depicts the correlated energy level diagram. The highly vibrationally excited Na_2 molecules $X^1\Sigma_g^+(v''=33, J''=11)$ and $X^1\Sigma_g^+(v''=45, J''=11)$ were realized via stimulated emission pumping, and the excited Na_2 states were then probed via LIF. While a YAG laser pulse of 532 nm was used to pump the Na_2 molecules from the $X^1\Sigma_g^+(v''=0, J''=11)$ state to the $A^1\Sigma_u^+(v' = 40, J' = 10)$ state [20], an OPO served as a dump laser (with wavelengths of 698 and 763 nm) to ensure that the Na_2 $A^1\Sigma_u^+(v' = 40, J' = 10)$ state was pumped back to the highly vibrationally excited $Na_2 X^1\Sigma_g^+(v'' = 33, J'' = 11)$ and $X^1\Sigma_g^+(v''=45, J''=11)$ states. A continuous-wave (CW) Ti:sapphire (Ti:Sa) laser was employed to probe either the vibrational state or the collisionally populated states of the prepared molecules.

Na_2 $X^1\Sigma_g^+(v''=33, J''=11)$ and $X^1\Sigma_g^+(v''=45, J''=11)$ states were excited to the $A^1\Sigma_u^+(v'=21, J'=10)$ state using 799.7 and 886.3 nm Ti:Sa lasers, respectively. The $A^1\Sigma_u^+(v'=21, J'=10)$ state of Na_2

relaxed to the $X^1\Sigma_g^+(v'' = 0\text{–}4)$ state, and LIF was detected using intensified charge-coupled device (ICCD) in the direction perpendicular to the laser propagation direction.

Figure 3 shows a segment of the LIF spectrum of the $A(v' = 21, J' = 10) \leftarrow X(v'' = 33, J'' = 11)$ band of Na_2, revealing that $J'' = 11$ of $v'' = 33$ of ground state Na_2 were prepared. The assignment of the spectrum could be easily performed since the molecular constants of Na_2 are known for both the upper and lower states. According to Fig. 3, the $v'' = 33$ state was excited by stimulated emission pumping (SEP).

3. Results and discussion

3.1. Density measurements of $Na_2(v'', J'')$ states

The power of the Ti:Sa laser was kept as small as 0.1 μW using neutral-density filters, and the beam diameter at the center of the cell was adjusted to 1 mm by means of a lens with a focal length of 1 meter and an aperture. The density of the $Na_2(v'', J'')$ states was measured by inducing the $X^1\Sigma_g^+(v'', J'') \rightarrow A^1\Sigma_u^+(v', J')$ transition with the Ti:Sa laser and monitoring its spread. The transmitted intensity $I_v(L)$ of the laser beam with frequency v after passing through the vapor of length L was calculated as follows [21]:

$$\frac{\Delta I}{I_v(0)} = 1 - \exp\left(-k_{v',J'\leftarrow v'',J''}(v)\ L\right), \tag{1}$$

where $\Delta I = I_v(0) - I_v(L)$; $I_v(0)$ is the incident intensity; and $k_{v',J'\leftarrow v'',J''}(v)$ is the absorption coefficient as a function of frequency. The number density of the $Na_2(v'', J'')$ states is related to the integral of the $k_{v',J'\leftarrow v'',J''}(v)$ function as [21]

$$\int dv\ k_{v',J'\leftarrow v'',J''}(v) =$$

$$\frac{(\lambda_{v',J'\leftarrow v'',J''})^2}{8\pi} \frac{g_{J'}}{g_{J''}} \left[Na_2(v'', J'')\right] \Gamma_{v',J'\rightarrow v'',J''}, \tag{2}$$

where $g_{J'}$ and $g_{J''}$ are the degrees of degradation of the J' and J'' states, respectively; $\Gamma_{v',J'\rightarrow v'',J''}$ is the natural radiation rate during the transition, and $\lambda_{v',J'\leftarrow v'',J''}$ is the wavelength of the transition.

Figure 4 depicts the time-resolved fluorescence semilogarithmic plot of the $A^1\Sigma_u^+(v' = 40, J' = 10) \rightarrow X^1\Sigma_g^+(v'' = 45, J'' = 11)$ transformation underwent by Na_2 upon the excitation of the $A(40, 10)$ state by the YAG laser. In the experiment, the relationship between ln(signal) and t is linear under single-collision conditions. Here, 0.6 μs is the time of a single collision, and multiple collisions after 0.6 μs do not obey the linear relationship. The representative number of data points is 40, and the step length varies (10 ns) based on the time scale of the profile. The slope of the fitting line yields the radiation rate.
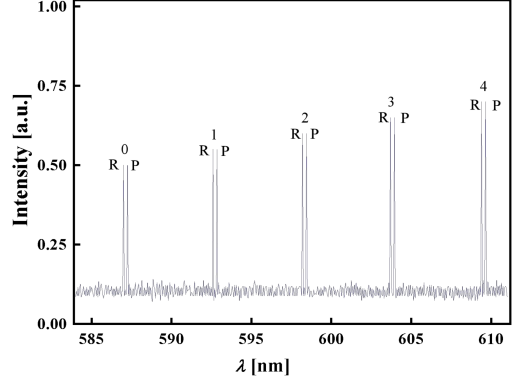

Fig. 3. Part of the dispersed fluorescence spectrum of the $A(21, 10) \leftarrow X(33, 11)$ band of Na_2, indicating that the $X(33, 11)$ ground state of Na_2 was prepared.
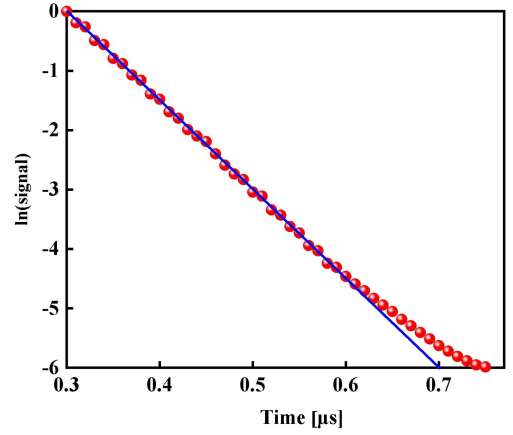

Fig. 4. Time-resolved fluorescence for the $A(40, 10) \rightarrow X(45, 11)$ transition of Na_2; the corresponding radiation rate is 1.5×10^7 s^{-1} ($T_{cell} = 670$ K).

TABLE I

Average densities of the $Na_2(v'' = 45, J'' = 11)$ states (in cm^{-3}) for different T_{cell} values. Note: The numbers in the parentheses denote the 2σ errors.

T_{cell} [K]	Na_2 (45, 11)
450	1.0(0.3)
523	2.1(0.6)
593	2.5(0.7)
670	3.3(0.8)
800	4.1(1.1)
900	4.9(1.3)

The nascent number density of the $Na_2(v'', J'')$ states was determined from the absorption measurements at $t = 1$ μs during excitation with an OPO laser. Absorption coefficients and transient Doppler-broadening linewidths were used to convert the absorbed signals into $Na_2(v'', J'')$ populations. The average densities of the $Na_2(45, 11)$ state for different T_{cell} values are listed in Table I.

In Table I, σ is the uncertainty that was calculated using Excel based on the standard deviation of the experimental data obtained from multiple measurements.

3.2. Vibration–rotation energy transfer

The initial population of CO_2 in the J state is depleted upon collision with the highly excited $Na_2(v'')$ state according to the following transition [22]

$$Na_2(v'') + CO_2(00^00, J) \xrightarrow{k_{dep}}$$

$$Na_2(v''-\Delta v'') + CO_2(00^00, J'). \tag{3}$$
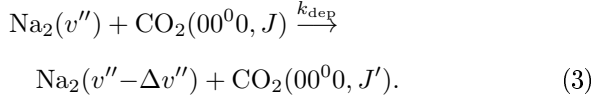
Simultaneously, the CO_2 molecules are scattered into the same J-state according to the transition below [22]

$$Na_2(v'') + CO_2(\text{cell temperature}) \xrightarrow{k_{app}^J}$$

$$Na_2(v''-\Delta v'') + CO_2(00^00, J). \tag{4}$$
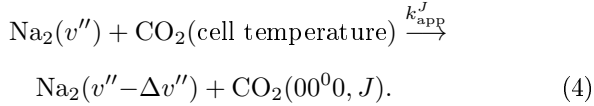
The population changes related to any collision that alters the initial state of rotation will cause depletion or appearance of J-specific for CO_2.

Nascent CO_2 populations are determined from the intensity of the transient overtone LIF line measured at short intervals of time relative to the period between collisions [11]. Before recording the LIF intensities, the filter is removed. At a pressure of 15 mTorr, the collision time is around 4 μs [6]. Thus, the transient intensity measurements were made at a time $t = 1$ μs, which is comparable to the average time of collisions between molecules. Such a short time corresponds to the scattered CO_2 molecule populations, making secondary quenching collisions impossible.

3.3. Rotational distribution of CO_2

The proportion of the population at a level specified by J can be written in terms of the ratio of the transient intensities before and after excitation of the $Na_2(v'')$ states, that is [23]

$$\frac{\left[CO_2(00^00, J)\right]_{t=1\,\mu s}}{\left[CO_2(00^00, J)\right]_{t=0}} = \frac{I_{t=1\,\mu s}^J}{I_{t=0}^J}, \tag{5}$$

where $[CO_2(00^00, J)]_{t=0}$ is determined by the Boltzmann distribution according to [23]

$$[CO_2(00^00, J)]_{t=0} = [CO_2]_0 \frac{B(2J+1)}{k_B T} e^{-\frac{BJ(J+1)}{k_B T}}, \tag{6}$$

in which $B = 0.394$ cm^{-1} is the rotational constant for CO_2. In turn, $I_{t=0}^J$ is the transient intensity before excitation of the $Na_2(v'')$ states, and $I_{t=1\,\mu s}^J$
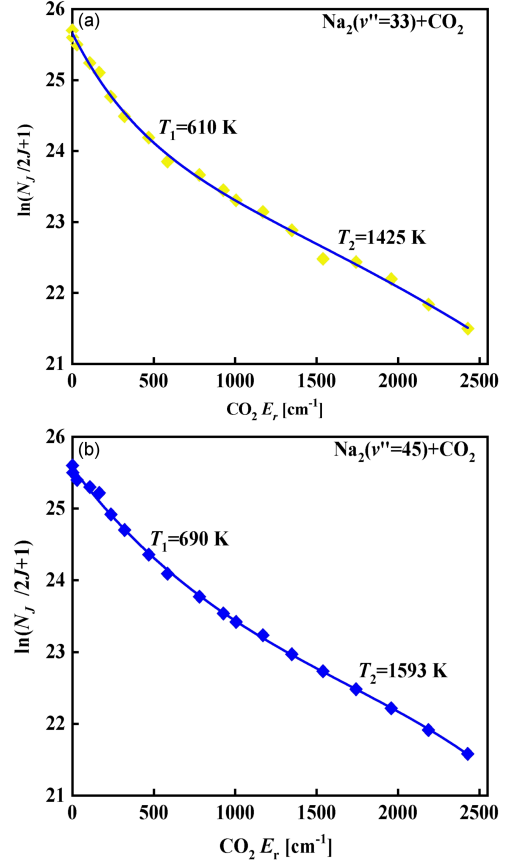

Fig. 5. Fitting of the nascent rotational distribution of CO_2 using the two-component biexponential model described in (7).

denotes the $(10^05, J)$–$(00^00, J)$ transition LIF intensity surveying at $t = 1$ μs. The time resolution of the LIF detection is 10 ns.

Figure 5 depicts the nascent rotation distribution of the scattered $CO_2(00^00)$ molecules in collisions with $Na_2(v'' = 33$ and $45)$ at $T_{cell} = 670$ K. A preferable profile of the nascent rotational distribution can be obtained using the sum of two separate distributions [10], that is [17]

$$\left[CO_2(J)\right] = (2J+1)\left(I_1 \exp\left(-\frac{BJ(J+1)}{k_B T_1}\right)\right.$$

$$\left. + I_2 \exp\left(-\frac{BJ(J+1)}{k_B T_2}\right)\right). \tag{7}$$

Here, T_1 and T_2 are the rotational temperatures, and I_1 and I_2 are the relative intensities.

For the collisions with $Na_2(v'' = 33)$, the fitting yields a low-energy distribution for $T_1 = 610 \pm 80$ K and a high-energy distribution for $T_2 = 1425 \pm 150$ K. For the collisions with $Na_2(v'' = 45)$, the CO_2 rotational temperatures are $T_1 = 690 \pm 90$ K and $T_2 = 1593 \pm 165$ K. The fact that T_1 is very close to the inception point of 670 K in the distribution suggests that nearly elastic collisions are responsible
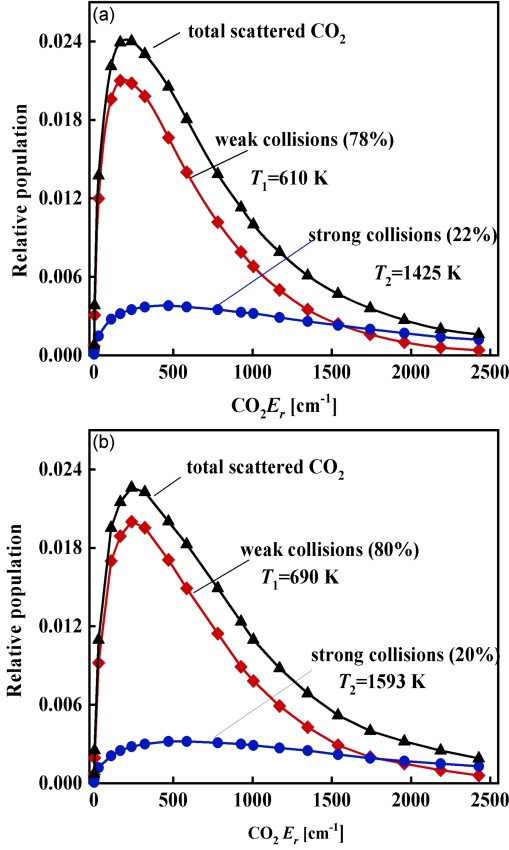
Fig. 6. Rotational distributions of the collisions with (a) $Na_2(v'' = 33)$ and (b) $Na_2(v'' = 45)$. For both $Na_2(v'')$ energies, the weak-collision pathway accounts for ~79% of all collisions with the $CO_2(00^00)$ products, while the strong-collision pathway accounts for ~21% of these collisions.

for populating the low-J final states. For comparison, the strong collisions that cause high-energy contrails are inelastic collisions causing a large increase in J.

Figure 6 depicts the rotational distribution for the collisions with the CO_2 and $Na_2(v'' = 33$ and 45) molecules. The combined strength of the weak-collision ingredient of CO_2 accounted for 79% of the total number of collisions, while the high-energy ingredient accounted for 21%. Therefore, nearly four-fifths of the collisions involved only small changes in the rotation of CO_2, while the remaining one-fifth of the collisions resulted in significant changes in the rotational energy.

3.4. Translational temperature of CO_2

The nascent distribution of the recoil velocity for strong collisions is determined based on the LIF line for each CO_2 rotational state. The shape of the LIF line for the $CO_2(00^00, J = 62)$ state is shown in Fig. 7.
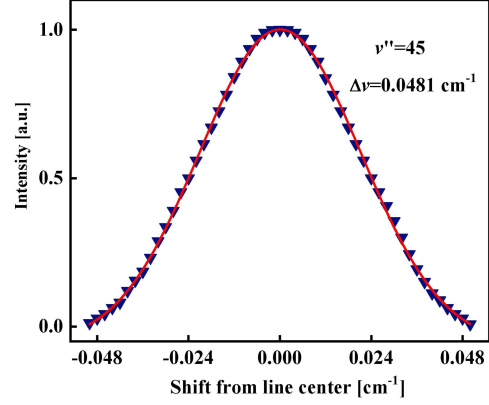

Fig. 7. Doppler-broadened transition line for $CO_2(00^00, J = 62)$ collected at $t = 1$ μs, following the excitation of $Na_2(v'' = 45)$ ($T_{cell} = 670$ K).
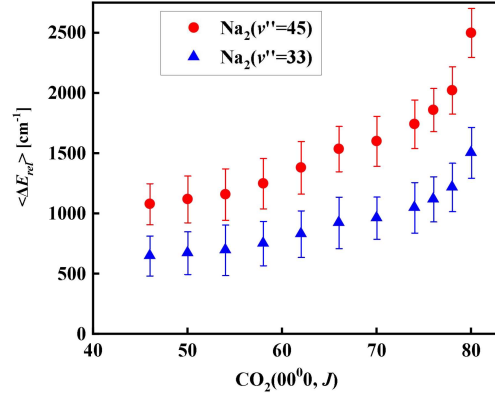

Fig. 8. Comparison of the nascent $\langle \Delta E_{rel} \rangle$ values for the products of the collisions between the CO_2 and $Na_2(v'')$ molecules.

The full width at half maximum of the linewidth was found to be $\Delta v = 0.0481$ cm^{-1}, which is equivalent to the velocity distribution of the laboratory frame at a translational temperature T_{trans} of 1348 ± 210 K. The temperature of the laboratory frame was determined as $T_{trans} = mc^2/(8k_B \ln(2))(\Delta v/v_0)^2$ [15], where the mass of CO_2 is denoted as m, and the rovibrational transition frequency at the line center is denoted as v_0. The translational temperature corresponding to the center of mass was determined from the following relationship [15]

$$T_{rel} = T_{trans} + \frac{m_{CO_2}}{m_{Na_2}}(T_{trans} - T_0), \qquad (8)$$

where T_0 is the temperature of the cell. The variation in the mean translational energy of the center of mass due to the collisions of $Na_2(v'')$ with CO_2 is defined as $\langle \Delta E_{rel} \rangle$ (in cm^{-1}). The values of $\langle \Delta E_{rel} \rangle$ can be established using the expression $\langle \Delta E_{rel} \rangle = 1.5k_B(T_{rel} - T_0)$. For $Na_2(v'' = 45)$, the temperature of the relative translational energy distribution for the $J = 62$ state of CO_2 is $T_{rel} = 2000 \pm 316$ K, which corresponds to $\langle \Delta E_{rel} \rangle = 1382 \pm 218$ cm^{-1}.
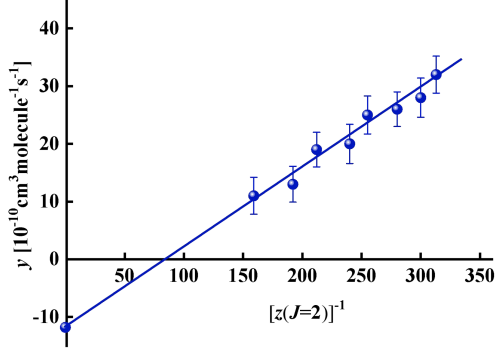
Fig. 9. Derivation of the rate constants $k_{app}^{J=2}$ and k_{dep} for the collisions between $Na_2(v'' = 45)$ and CO_2. The slope of the fitted line yields $k_{app}^{J=2} = (1.4 \pm 0.3) \times 10^{-11}$ cm^3/(molecule s). The intercept yields $k_{dep} = (11.8 \pm 3.4) \times 10^{-10}$ cm^3/(molecule s).

TABLE II

Energy transfer rate constants k_{app}^J for the collisions between $Na_2(v'')$ and CO_2. Note: This table represents a portion of the k_{app}^J values.

J	$k_{app}^J \times 10^{-12}$ [cm^3/(molecule s)]	
	$Na_2(v'' = 33)$	$Na_2(v'' = 45)$
2	28 ± 6	14 ± 3
8	39 ± 8	29 ± 6
22	62 ± 13	56 ± 12
28	21 ± 5	26 ± 6
34	16 ± 4	24 ± 5
40	12 ± 3	8.1 ± 1.7
46	8.3 ± 1.7	7.2 ± 1.5
58	7.6 ± 1.6	5.6 ± 1.2
64	5.3 ± 1.1	4.2 ± 0.9
70	1.5 ± 0.3	0.9 ± 0.2
78	1.1 ± 0.2	0.7 ± 0.2

The nascent energy dependence $\langle \Delta E_{rel} \rangle$ values of the $J = 46$–80 states after a single collision between the CO_2 and $Na_2(v'')$ molecules with the vibrational states 33 and 45 are shown in Fig. 8. When the $Na_2(v'')$ energy is high enough, the recoil energy of all J states also increases. The amount of energy converted to the translational energy rises with the donor energy. It was found that for every 25% increase in donor vibrational energy, the translational energy of a J-specific collision product increased by at least 60%.

3.5. Appearance and depletion rate constants

As shown in Fig. 5, the energy transfer rates of the J-state distribution determining the nascent appearance of some product states can be established according to (4) by combining the rate measurements and relative population experiments. In turn,

TABLE III

Rate constants corresponding to the depletion of the $CO_2(00^00, J)$ states due to the collision with $Na_2(v")$.

J	$k_{dep} \times 10^{-10}$ [cm^3/(molecule s)]	
	$Na_2(v'' = 33)$	$Na_2(v'' = 45)$
2	12.1 ± 3.5	11.8 ± 3.4
8	10.5 ± 3.1	9.7 ± 2.8
22	9.6 ± 2.8	8.8 ± 2.6
28	8.5 ± 2.5	5.3 ± 1.5
34	3.2 ± 1.0	2.7 ± 0.8
38	1.3 ± 0.4	1.1 ± 0.3
$\langle k_{dep} \rangle$	7.5 ± 2.2	6.6 ± 1.9

the J-specific rate constant k_{app}^J for the appearance of the $CO_2(00^00, J)$ state is defined as [18]

$$\Delta\left[CO_2(00^00, J)\right]_{app} = k_{app}^J \ [CO_2]_0 \ [Na_2(v'')]_0 \Delta t, \tag{9}$$

where $\Delta[CO_2(00^00, J)]_{app}$ is the appearance population with an initial $Na_2(v'')$ concentration of $[Na_2(v'')]_0$ states and an initial CO_2 population of $[CO_2]_0$ states; $\Delta t = 1 \ \mu s$.

The depletion rate of CO_2 in a given state is described as [18]

$$\Delta \ [CO_2(00^00, J)]_{dep} =$$
$$-k_{dep} z(J) [CO_2]_0 \ [Na_2(v'')]_0 \Delta t, \tag{10}$$

where k_{dep} is the depletion rate constant, and $z(J)$ is the fraction of CO_2 in a particular J-state. Using the first-order approximation, it is assumed that the depletion rate constant is independent of J.

By combining (9) and (10), it can be found that [18]

$$\frac{\Delta \ [CO_2(J)]_{dep} + \Delta[CO_2(J)]_{app}}{[CO_2(J)]_0 \ [Na_2(v'')]_0 \Delta t} = -k_{dep} + k_{app}^J z(J)^{-1}, \tag{11}$$

where $z(J)^{-1} = [CO_2]_0/[CO_2(J)]_0 = \left[B(2J+1)/(k_B T) \times \exp(-BJ(J + 1)/(k_B T))) \right]^{-1}$, T is the temperature in the cell, and $\Delta t = 10^{-6}$ s. By substituting the observed LIF intensity for the population in (11), it is evident that [18]

$$y = \frac{10^6}{[Na_2(v'')]} \frac{I_0^J - I_{t=1 \mu s}^J}{I_0^J} = -k_{dep} + k_{app}^J z(J)^{-1}. \tag{12}$$

Figure 9 depicts the functional relationship between the left-hand side of (12) and $z(J)^{-1}$ as a straight line with a slope of k_{app}^J and an intercept of $-k_{dep}$. Tables II and III contain the measured k_{app}^J and k_{dep} values, respectively. The uncertainties in Tables II and III are treated the same way as the uncertainties in Table I.

The sum of the rate constants k_{app}^J ($k_{app} = \Sigma k_{app}^J$) was used to determine the apparent rate constants of all CO_2 product states. For the collisions with $Na_2(v'' = 33)$, it was found that $k_{app} = (8.0 \pm 2.1) \times 10^{-10}$ cm^3/(molecule s). This result

is comparable to that obtained for $Na_2(v'' = 45)$, for which the appearance rate constant is $k_{app} = (6.9 \pm 1.8) \times 10^{-10}$ cm^3/(molecule s). For the collisions with $Na_2(v'' = 33)$, the mean depletion rate of a low-J state is $(7.5 \pm 2.2) \times 10^{-10}$ cm^3/(molecule s), which also approaches the depletion rate constant obtained for $Na_2(v'' = 45)$, namely $\langle k_{dep} \rangle = (6.6 \pm 1.9) \times 10^{-10}$ cm^3/(molecule s). The uniformity of the overall depletion and appearance rates for the two separate Na_2 energies indicates the significance of the V-RT energy transfer and confirms the fact that the collision rate constant of the system does not change with the donor energy.

4. Conclusions

The excitation of Na_2 molecules to the vibrational states $v'' = 33$ and $v'' = 45$ was realized using SEP. The full-state resolved $CO_2(00^0, J)$ molecules were produced when the excited Na_2 ($v'' = 33$ and 45) collided with $CO_2(00^00)$, exhibiting a biexponential rotational distribution. The biexponential distribution of the scattered CO_2 molecules indicated that 79% of the collisions were weakly inelastic, which had a minimal impact on the rotational motion of CO_2 upon scattering. The remaining collisions (21%) were strongly inelastic, and their higher energies significantly altered the rotational energy of CO_2. It was found that for every 25% increase in donor vibrational energy, the translational energy of the J-specific collision product increased by 60% or more. The calculated average depletion and appearance rate constant for the collisions of $Na_2(v'' = 33$ and 45) with $CO_2(00^00)$ were calculated to be $(7.5 \pm 2.2) \times 10^{-10}$ and $(6.6 \pm 1.9) \times 10^{-10}$ cm^3/(molecule s), respectively.

Acknowledgments

References

[1] F.J. Domínguez-Gutiérrez, P.S. Krstić, R. Cabrera-Trujillo, *Adv. Quant. Chem.* **71**, 353 (2015).

[2] D. Gust, M. Scholz, K. Oum, T. Lenzer, *Molecules* **28**, 7841 (2023).

[3] R. J. Liu, X. Y. Shen, D. C. Wang, *Anal. Chem.* **93**, 7394 (2021).

[4] E. Solmaz, D. Levko, L. L. Raja, *AIP Adv.* **13**, 065009 (2023).

[5] A. Starikovskiy, N. Aleksandrov, A. Rakitin, *Philos. Trans. R. Soc. A* **37**, 740 (2012).

[6] A. J. McCaffery, *Philos. Ttans. R. Soc. A* **376**, 20170150 (2018).

[7] D. J. Donaldson, M. Ammann, T. Bartels-Rausch, U. Pöschl, *J. Phys. Chem. A* **116**, 6312 (2012).

[8] R. Samii, A. Fransson, P. Mpofu, P. Niiranen, L. Ojamäe, V. Kessler, N. J. O'Brien, *Inorg. Chem.* **61**, 20804 (2022).

[9] P.H. Paul, J.A. Gray, J.L. Durant Jr., J.W. Thoman Jr., *Appl. Phys. B Lasers Opt.* **57**, 249 (1993).

[10] B. Nikoobakht, *J. Chem. Phys.* **157**, 014101 (2022).

[11] M.R. Laskowski, T.J. Michael, H.M. Ogden, M.H. Alexander, A.S. Mullin, *Faraday Discuss.* **238**, 87 (2022).

[12] D.H. Zhu, B. Zhang, Y.F. Shen, K. Dai, *Chin. Phys. Lett.* **9**, 112 (2011).

[13] M. Morgenroth, T. Lenzer, K. Oum, *J. Phys. Chem. C* **127**, 4582 (2023).

[14] S. Hoshino, O. Yamamoto, K. Tsukiyama, *ACS Omega* **7**, 3605 (2022).

[15] L.W. Yuan, J. Du, A.S. Mullin, *J. Chem. Phys.* **129**, 014303 (2008).

[16] D.K. Havey, J. Du, Q.N. Liu, A.S. Mullin, *J. Phys. Chem. A* **114**, 1569 (2010).

[17] J. Du, N.A. Sassin, D.K. Havey, K. Hsu, A.S. Mullin, *J. Phys. Chem. A* **117**, 12104 (2013).

[18] X.Y. Shen, S.Y. Wang, K. Dai, Y.F. Shen, *Spectrochim. Acta A* **173**, 516 (2017).

[19] X.H. Cui, B.X. Mu, Y.F. Shen, K. Dai, *J. Quant. Spectrosc. Radiat. Transfer* **113**, 2081 (2012).

[20] K.P. Huber, G. Herzberg, *Molecular Spectra and Molecular Structure IV. Constants of Diatomic Molecules* Van Nostrand Reinhold, 1979, p. 432.

[21] X.Y. Shen, S.Y. Wang, K. Dai, Y.F. Shen, A.J. McCaffery, *J. Chem. Phys.* **146**, 114307 (2017).

[22] M.C. Wall, B.A. Stewart, A.S. Mullin, *J. Chem. Phys.* **108**, 6185 (1998).

[23] A. Alghazi, J. Liu, K. Dai, Y.F. Shen, *Spectrosc. Spectral Anal.* **36**, 1317 (2017).